

Unified trend of superconducting transition temperature versus Hall coefficient for ultrathin FeSe films prepared on different oxide substrates

Junichi Shioyai,* Tomoki Miyakawa, Yukihiro Ito, Tsutomu Nojima, and Atsushi Tsukazaki
Institute for Materials Research, Tohoku University, Sendai 980-8577, Japan

(Received 10 October 2016; published 1 March 2017)

High transition temperature (T_c) superconductivity in FeSe/SrTiO₃ has been widely discussed on the possible mechanisms in conjunction with the various effects of interface between FeSe and SrTiO₃ substrate. By employing an electric-double-layer transistor configuration, which enables both the electrostatic carrier doping and electrochemical thickness tuning, we investigated the interfacial effect on the high- T_c phase at around 40 K in FeSe films deposited on SrTiO₃, MgO, and KTaO₃ substrates. The systematic study on thickness dependence of transport properties under a certain gate voltage reveals the universal trend of the onset T_c against the Hall coefficient in all the FeSe films, irrespective of the substrate materials in which the different contribution of interfacial effect is expected. The independence of the highest T_c on substrate materials evidences that the high- T_c superconductivity at around 40 K does not primarily originate from a specific interface combination but from a charge carrier filling at specific electronic band structure.

DOI: [10.1103/PhysRevB.95.115101](https://doi.org/10.1103/PhysRevB.95.115101)

I. INTRODUCTION

Interface superconductivity has been explored for its exotic pairing mechanism [1–4], and for potential controllability using electric field [5,6] or interface engineering [7,8]. The recent discovery of high transition temperature (high- T_c) superconductivity in monolayer (ML) iron selenide (FeSe) [9] is on the track of these prospects, boosting the fascinating effect at the interface between FeSe and oxides [10–12]. Based on the insights from scanning tunneling spectroscopy [10] and angle-resolved photoemission spectroscopy (ARPES) [11–13] revealing the superconducting (SC) gap closing temperature as high as 65 K, the suggested interfacial effects of FeSe/SrTiO₃ on its high- T_c superconductivity involve charge transfer from substrate [11,14,15] and modulation of electronic structure of FeSe [13,16]. In addition, electron-phonon coupling between FeSe and SrTiO₃ [12,17] and in-plane tensile strain [18,19] are proposed to play a role. In contrast to the gap measurements, the onset T_c (T_c^{on}) in transport measurements has reached about 40 K for various configurations including FeTe/Si-capped 1 ML FeSe on SrTiO₃ [10,20–22], electric-double-layer (EDL) transistor with FeSe/SrTiO₃ [23,24], FeSe/MgO [23], and single crystal flakes on SiO₂/Si [25]. In particular, the experiments of electrostatic doping in such EDL transistors point out the importance of the electron accumulation and/or band bending for inducing high- T_c superconductivity at about 40 K [23]. However, since the mismatch between 65 K from *in situ* gap measurement and 40 K from *ex situ* transport measurement is still under debate, it has not been resolved what plays the most central role to high- T_c superconductivity in FeSe on oxide substrates [12].

In cuprate superconductors, the Hall effect measurement at the normal state has provided intuitive understanding of the electronic phase involving high- T_c superconductivity in different doping concentrations [26,27]. Similarly, in the case of Fe-based superconductors, it is important to clarify the link between the superconducting and the normal electronic

states with different doping levels for deeper understanding of its origin [28,29]. Especially, FeSe is a particular system characterized with small Fermi surfaces in bulk single crystals, exhibiting a BCS-BEC crossover [30]. However, the Fe-based superconductors generally possess a semimetallic electronic structure; with hole pocket at the Γ point and electron pocket at the M point, which makes analyzing Hall effect more difficult. In this study, by combining the Hall effect measurements with electrochemical etching in the FeSe-based EDL transistor (FeSe-EDLT) configuration shown in Fig. 1(a), we found a universal trend of T_c^{on} as a function of the Hall coefficient in normal state at 50 K regardless of oxide substrate materials. In addition, we quantitatively extracted the thicknesses of charge accumulation layers at the ionic liquid (IL)/FeSe interface (d_{EDL}) and of charge transfer layers at the FeSe/oxide substrate interface (d_{CT}) [Fig. 1(b)]. Our finding recalls the importance of charge transfer among the variety of interfacial effects as well as electrostatic tuning of charge balance in FeSe-EDLT.

II. EXPERIMENTAL DETAILS

In this study, we employed SrTiO₃ (001), MgO (001), and KTaO₃ (001) insulating substrates for transport measurements of FeSe thin films. The epitaxial FeSe films with thickness $d = 14.0$, 10.4 , and 26.7 nm were deposited on SrTiO₃, MgO, and KTaO₃, respectively, by pulsed-laser deposition at the substrate temperature of 300 °C. After the growth, the films were annealed *in situ* at 450 °C for 30 minutes to obtain better metallic transport properties [23]. There is no clear difference in FeSe film quality on different substrate materials as confirmed by rocking curve of FeSe (001) x-ray diffraction peak and atomic force microscopy. Figure 1(c) shows an optical micrograph of the Hall-bar-shaped FeSe-EDLT, which was formed using the metal shadow mask during deposition. Indium pads and a platinum film were used as Ohmic contact electrodes and a side gate electrode, respectively. All the indium pads were covered with silicone sealant to prevent any possible chemical reaction with IL. Finally, IL, N,N -diethyl- N -methyl- N -(2-methoxyethyl)ammonium

*junichi.shioyai@imr.tohoku.ac.jp

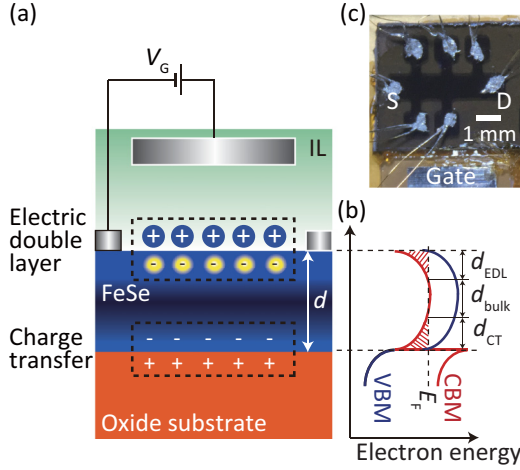


FIG. 1. (a) Schematics of layer geometry of FeSe-EDLT on oxide substrate and (b) corresponding conduction band minimum (CBM, solid red line) at the M point and valence band maximum (VBM, solid blue line) at the Γ point. The length scales d , d_{bulk} , d_{EDL} , and d_{CT} indicate thicknesses of total FeSe film, bulky middle layer, electron-rich layers from EDL, and from substrate, respectively. (c) Optical micrograph of FeSe-EDLT with Hall bar geometry. S and D stand for source and drain electrodes.

bis(trifluoromethanesulfonyl)imide, was put on the channel and gate electrode. The sheet resistance (R_s) was measured by standard four-terminal method. The gate voltage (V_G) was applied using source-measure unit while simultaneously measuring gate leakage current (I_G). As reported in Ref. [23], we can perform both the electrostatic carrier tuning and

electrochemical etching using this type of EDLT device by precisely tuning the sample temperature (T). While T was kept at 220 K to control the doping level without etching, T was increased at around 240 K while keeping V_G at 5 V to induce the electrochemical etching. R_s - T curves were measured after each etching cycle or after each electrostatic discharging event. The Hall effect measurements were done in the normal state at $T = 50$ K in the perpendicular magnetic field (B) ranging from -9 T to $+9$ T. The film thickness for each R_s - T curve was calibrated by the temporal integration of I_G under the assumption that the etching rate was proportional to I_G [23]. The error value of thickness was defined by the initial surface roughness, which was almost equal to the etch-stopped surface roughness [23].

III. RESULTS AND DISCUSSION

Figures 2(a)–2(f) show the T dependence of the normalized R_s (top panels) at $B = 0$ T and B dependence of the Hall resistance (R_{Hall}) at $T = 50$ K (bottom panels) of FeSe-EDLTs on SrTiO₃ [Figs. 2(a) and 2(d)], MgO [Figs. 2(b) and 2(e)] and KTaO₃ [Figs. 2(c) and 2(f)] at different thickness. All the films exhibit clear SC transitions with zero resistance when the films are thinner than certain critical thicknesses. The overall trend of thickness dependence in FeSe/SrTiO₃ and FeSe/MgO is consistent with the previous report [23]; T_c^{on} at about 40 K appears in a thicker condition than 1 ML (~ 0.6 nm). In addition, we observe that the R_s - T curve for FeSe-EDLT on KTaO₃ shows SC transition reaching zero resistance at very thick 25 nm with $T_c^{\text{on}} \sim 20$ K as shown in Fig. 2(c).

As for the Hall effect measurements in Figs. 2(d)–2(f), the sign of Hall coefficient [$R_H = (R_{\text{Hall}}/B)d$] is initially positive

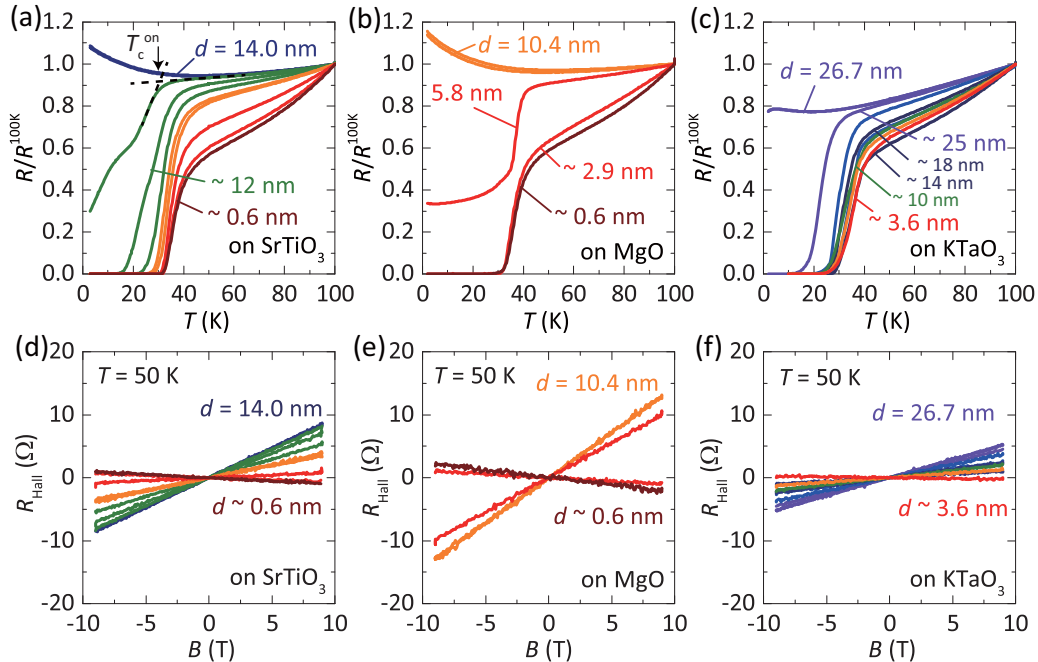


FIG. 2. Normalized sheet resistance with respect to $T = 100$ K (denoted $R/R^{100\text{K}}$) as a function of temperature for FeSe on (a) SrTiO₃, (b) MgO, and (c) KTaO₃ substrates. The arrow in Fig. 2(a) indicates the T_c^{on} at which extrapolated lines from the normal state and the superconducting transition region intersect. The corresponding Hall resistance R_{Hall} measured at $T = 50$ K are shown for FeSe on (d) SrTiO₃, (e) MgO, and (f) KTaO₃ substrates. Color code reflects film thickness.

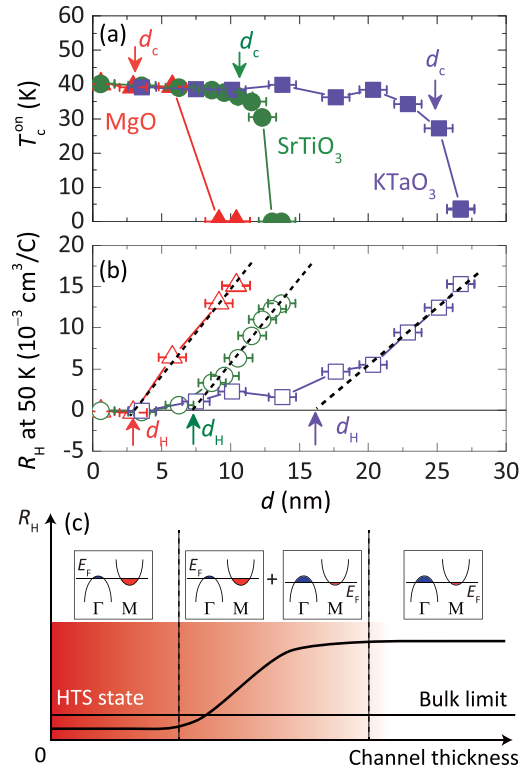


FIG. 3. Thickness dependence of (a) T_c^{on} and (b) R_H at $T = 50$ K for the FeSe-EDLT on SrTiO₃ (green), MgO (red), and KTaO₃ (purple) substrates. (c) (Top) Schematic image of electronic band structure of FeSe film at different thickness regions. (Bottom) A sketch of thickness dependence of R_H for FeSe-EDLT in this study.

for all the films, indicating the contribution of hole carriers dominates the conduction even under $V_G = 5$ V. However, the slope of R_{Hall} gradually varies from positive to negative against thickness reduction. The positive slope at the thick condition implies that the FeSe film behaves like bulk with the carrier density in hole pocket at the Γ point being higher than that in electron pocket at the M point [31]. In contrast, the sign change in R_H in the thinner condition evidences that the dominant carrier type converts to electron. By taking $R_H \sim -0.33 \text{ cm}^3/\text{C}$ for 2.9-nm-thick FeSe on MgO, the electron concentration extracted in the usual manner $n = 1/R_{\text{He}}$ is $1.9 \times 10^{22} \text{ cm}^{-3}$. This value agrees well with the transport data at 50 K previously reported in the FeTe/Si-capped 1 ML FeSe/SrTiO₃ [22], which strongly depends on measurement temperature. R_H in FeSe may not reflect the actual carrier density as discussed on strong temperature dependence of cuprates [32,33]. As far as we applied B up to ± 9 T, the nonlinear R_{Hall} , typical two-band behavior, was not observed, indicating that the semimetallic feature is not confirmed in our measurements.

T_c^{on} obtained from Figs. 2(a)–2(c) and R_H from Figs. 2(d)–2(f) are summarized in Figs. 3(a) and 3(b) as a function of film thickness, respectively. T_c^{on} is defined as the temperature at which extrapolated lines from the normal state and the superconducting transition intersect as indicated in Fig. 2(a). As shown in Fig. 3(a), T_c^{on} increases toward a saturated value at about 40 K with reducing the thickness for all the substrates. Note that $R_s(T)$ in the initial thick condition with

applying $V_G = 5$ V shows no sign of high- T_c SC, implying the electron accumulation layer under the gate voltage does not solely exhibit zero resistance [23]. The critical thickness d_c for observing zero resistance with high- T_c phase depends on substrate materials. As presented in Figs. 2(a) and 2(b), the R_s - T curves after the first etching did not show zero resistance at $d \sim 13$ nm and ~ 5.8 nm for FeSe-EDLTs on SrTiO₃ and MgO substrates, respectively. Further thickness reduction develops the superconductivity to exhibit zero resistance at $d \sim 12$ nm and ~ 2.9 nm. Therefore, d_c resides between these values. Here, we determined $d_c \sim 12 \pm 1.0$ nm for SrTiO₃, $\sim 4.5 \pm 1.0$ nm for MgO. These values are consistent with those in the previous work within thickness error bars: d_c is 9.6 ± 1.0 nm for SrTiO₃ and 5.9 ± 1.0 nm for MgO substrates [23]. However, high- T_c superconductivity in the FeSe-EDLT on KTaO₃ was observed after the first etching. This implies that $d_c \sim 26 \pm 1.0$ nm for FeSe film on KTaO₃ is only lower limit and it may be thicker than that estimated in Fig. 3(a) when the initial film is thicker. Each different film thickness was intentionally designed after preliminary experiments for roughly estimating d_c . As shown in Fig. 3(b), R_H at 50 K monotonically decreases with reducing thickness and finally its sign is reversed to negative value at $d = d_H$. It is revealed that the linear slopes of R_H - d (dotted lines) shows an almost constant value in three samples although thickness region is different.

The behavior of the R_H - d curve can be interpreted with the modification of the charge distribution along the film thickness as illustrated in Figs. 1(b) and 3(c). Under the application of V_G , R_H detects the sum of electron conduction in the top and bottom layers with the thickness d_{EDL} and d_{CT} , respectively, and hole conduction in the middle bulky layer d_{bulk} . In a thick condition ($d \gg d_{\text{EDL}} + d_{\text{CT}}$), the semimetallic bulk characteristics govern the positive R_H [right of Fig. 3(c)]. The reduction of thickness modulates the relative contributions of electron-rich and hole-rich layers, so that the measured R_H consists of the averaged signals from both the contributions in the medium thickness region [center of Fig. 3(c)]. Then, in the thin region ($d \leq d_{\text{EDL}} + d_{\text{CT}}$), the electrons at the M point become dominant carriers [left of Fig. 3(c)]. In this picture, the reduction of R_H with constant slope consequently indicates that the bulky hole-rich region d_{bulk} is effectively reduced with no variation of d_{EDL} and d_{CT} during etching under the constant V_G . In other words, the constant slope evidences that electronic property of bulky FeSe region on three samples is reliably reproducible at the identical film growth conditions.

T_c^{on} are plotted in Fig. 4 against R_H at 50 K to exemplify the relationship. A unified trend of T_c^{on} against R_H is clearly observed although each data point corresponds to different film thickness on three substrates in Figs. 3(a) and 3(b). The highest T_c^{on} at 40 K is achieved when R_H becomes close to zero or negative. This plot evidences that a certain amount of electron accumulation universally induces the superconductivity at 40 K under the same V_G , regardless of film thickness and substrate materials. It turns out that the high- T_c superconductivity links to charge balance in FeSe films. Unfortunately, the detail electron/hole filling cannot be discussed due to the linear R_{Hall} - B curve in this work. Therefore, much higher magnetic fields may provide a detailed picture of charge filling situation.

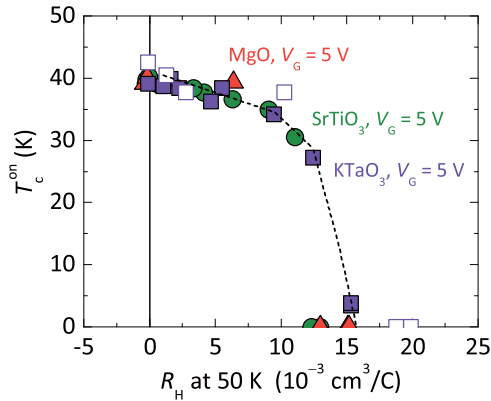


FIG. 4. T_c^{on} as a function of R_H at $T = 50$ K for FeSe-EDLT on SrTiO₃ (filled green circles), MgO (filled red triangles), and KTaO₃ (filled purple squares). The data for another FeSe-EDLT on KTaO₃ during etching before the discharging experiments presented in Fig. 5 is also plotted (open purple squares).

We also performed discharging experiments by removing V_G in fixed FeSe thickness to compare $T_c^{\text{on}}-R_H$ relationship in electrostatic mean. The experiments were conducted for 1-nm-thick FeSe on KTaO₃ in Figs. 5(a) and 5(b) and 2.9-nm-thick FeSe on MgO in Figs. 5(c) and 5(d). For the KTaO₃ substrate, the negative slope in the initial $R_{\text{Hall}}-B$ curve with $V_G = 5$ V (red) remains even after removing V_G to zero (purple) as shown in Fig. 5(b). The results elaborate the presence of the charge transfer from KTaO₃ substrate. In contrast, the 2.9-nm-thick FeSe on MgO shows clear superconductor-to-insulator transition by removing V_G to zero as shown in Fig. 5(c). Here, we chose 2.9-nm-thick condition because of just thinner than d_H . The negative slope in the initial $R_{\text{Hall}}-B$ curve (red) with electron-dominated conduction under

$V_G = 5$ V gradually converts to positive value with removing V_G , implying the hole-dominated conduction recovers. This result supports our suggestion that the charge transfer from MgO substrate can be ignored and the electrostatic electron accumulation at IL/FeSe interface dominates the transport and superconductivity [23].

Figure 5(e) summarized the data for 1-nm-thick FeSe on KTaO₃ (open purple squares) and 2.9-nm-thick FeSe on MgO (open red triangles) in discharging experiments. For comparison, the previous electrostatic studies in 10-nm-thick FeSe-EDLT on SrTiO₃ [24] (filled gray squares) are presented. Linear dependence of the $T_c^{\text{on}}-R_H$ curves in 1-nm-thick FeSe-EDLT on KTaO₃ and 2.9-nm-thick FeSe-EDLT on MgO in this study is similar to the 10-nm-thick FeSe-EDLT on SrTiO₃ substrate. This is a stark contrast to the universal trend in Fig. 4. The difference may come from the different origin of the measured R_H ; the charge balance of hole-rich and electron-rich layers changing with thickness (Fig. 4) and the balance of hole- and electron-band contributions changing with the Fermi energy or V_G [Fig. 5(e)], although in both cases, the band bending effect induces the high- T_c superconductivity at around 40 K in FeSe.

Finally, we address the length scale of the charge distribution in FeSe-EDLT. The comparison of d_c and d_H among three different substrate materials as shown in Fig. 3 allows a rough estimation of $d_{\text{EDL}}, d_{\text{CT}}$, and the SC order parameter penetration lengths due to the proximity effect, ξ_N^{EDL} and ξ_N^{CT} , from the top and bottom electron-rich layers, respectively, according to the following assumptions. (1) The sign change in R_H at 50 K occurs in $d < d_H = d_{\text{EDL}} + d_{\text{CT}}$ when whole film is governed with the electron-rich layer. (2) The zero resistance is observed in $d < d_c = d_{\text{EDL}} + \xi_N^{\text{EDL}} + d_{\text{CT}} + \xi_N^{\text{CT}}$ when the whole thickness contributes the high- T_c SC phase. In the case of MgO, it is plausible that $d_H = d_{\text{EDL}}$ owing to no charge transfer from substrate. Therefore, we can first define

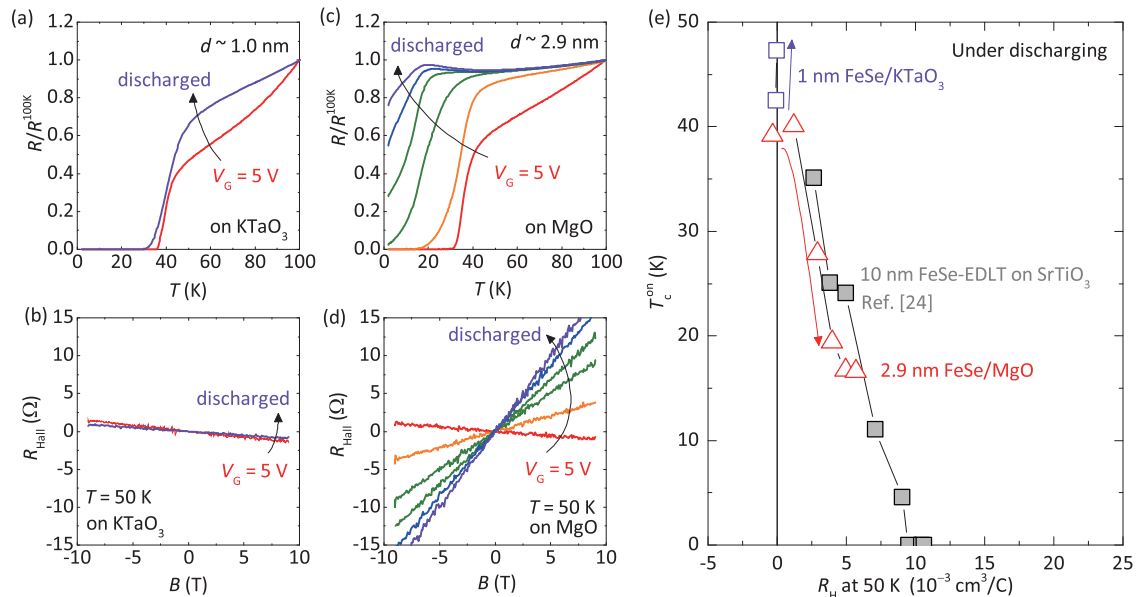


FIG. 5. (a) $R/R^{100\text{K}}-T$ curves for discharging experiments for 1.0-nm-thick FeSe on KTaO₃. (b) The corresponding Hall resistance measured at $T = 50$ K. (c), (d) The same data set for 2.9-nm-thick FeSe on MgO. Color code reflects the degree of discharging. (e) $T_c^{\text{on}}-R_H$ curve for discharging experiments on 2.9-nm-thick FeSe/MgO (open red triangles) and 1.0-nm-thick FeSe/KTaO₃ (open purple squares). Arrows indicate the direction of removing V_G . For comparison, the data for 10-nm-thick FeSe EDL transistor [24] (filled gray squares) are also plotted.

$d_{\text{EDL}} \sim 3$ nm for all the films. As for the FeSe on SrTiO₃, $d_{\text{H}} = d_{\text{CT}}(\text{STO}) + d_{\text{EDL}} = 7$ nm with the presence of charge transfer at the bottom interface, leading to $d_{\text{CT}}(\text{STO}) \sim 4$ nm. To apply the same analysis to the data set in KTaO₃, we estimate $d_{\text{H}} \sim 16$ nm by extrapolation of the positive slope to $R_{\text{H}} = 0$, resulting in $d_{\text{CT}}(\text{KTO}) \sim 13$ nm. Such thick $d_{\text{CT}}(\text{KTO})$ may originate from a large amount of charge transfer by polar discontinuity at the interface between (TaO₂)⁺ surface [34,35] and nonpolar FeSe and/or by the efficient band bending effect originating from the different work functions of KTaO₃ and FeSe [36]. The last issue to be discussed is the SC order parameter penetration length. Using $d_{\text{EDL}} \sim 3$ nm and $d_{\text{c}} \sim 4.5$ nm for MgO in the absence of charge transfer, $\xi_{\text{N}}^{\text{EDL}} \sim 1.5$ nm. When applying $d_{\text{EDL}} + \xi_{\text{N}}^{\text{EDL}} \sim 4.5$ nm to SrTiO₃ and KTaO₃, we obtain $\xi_{\text{N}}^{\text{CT}}(\text{STO}) \sim 3.5$ nm and $\xi_{\text{N}}^{\text{CT}}(\text{KTO}) > 8.5$ nm. It is plausible that $\xi_{\text{N}}^{\text{CT}}$ monotonically increases with increase in d_{CT} . The obtained $\xi_{\text{N}}^{\text{CT}}(\text{STO})$ is larger than that below 2 ML supposed by ARPES measurements [15]. This indicates that the band bending effect by IL gating enhances the $\xi_{\text{N}}^{\text{CT}}(\text{STO})$ and critical thickness exhibiting high- T_{c} superconductivity.

IV. CONCLUSION

In conclusion, we investigated the substrate material dependence of superconducting properties in FeSe-EDLT to exemplify the interfacial effects at FeSe/oxides. A universal trend between T_{c}^{on} and R_{H} at 50 K indicates significance of charge balance in the sample to obtain high- T_{c} superconductivity in FeSe films. The dependence of critical thickness d_{c} on substrate indicates that the length scale of charge transfer into FeSe strongly depends on substrate material. Our findings draw up a guideline to expand the interface (two-dimensional) into bulk (three-dimensional) superconductivity within the films by introducing electric field and interface engineering.

ACKNOWLEDGMENTS

This work was partly supported by Grant-in-Aid for Specially Promoted Research (No. KAKENHI 25000003), Young Scientists (A) (No. KAKENHI 16H05981) and Challenging Exploratory Research (No. KAKENHI 15K13354) from the Japan Society for the Promotion of Science (JSPS).

-
- [1] V. L. Ginzburg, *Phys. Lett.* **13**, 101 (1964).
 [2] V. L. Ginzburg, *J. Exptl. Theoret. Phys. (USSR)* **47**, 2318 (1964) [*Sov. Phys. JETP* **20**, 1549 (1965)].
 [3] W. A. Little, *Phys. Rev.* **134**, A1416 (1964).
 [4] S. Gariglio, M. Gabay, J. Mannhart, and J.-M. Triscone, *Physica C* **514**, 189 (2015).
 [5] C. H. Ahn, J.-M. Triscone, and J. Mannhart, *Nature (London)* **424**, 1015 (2003).
 [6] N. Reyren, S. Thie, A. D. Caviglia, L. Fitting Kourkoutis, G. Hammer, C. Richter, C. W. Schneider, T. Kopp, A.-S. Rüetschi, D. Jaccard, M. Gabay, D. A. Muller, J.-M. Triscone, and J. Mannhart, *Science* **317**, 1196 (2007).
 [7] K. Murase, S. Ishida, S. Takaoka, and T. Okimura, *Surf. Sci.* **170**, 486 (1986).
 [8] A. Gozar, G. Logvenov, L. Fitting Kourkoutis, A. T. Bollinger, L. A. Giannuzzi, D. A. Muller, and I. Bozovic, *Nature (London)* **455**, 782 (2008).
 [9] F. C. Hsu, J. Y. Luo, K. W. Yeh, T. K. Chen, T. W. Huang, P. M. Wu, Y. C. Lee, Y. L. Huang, Y. Y. Chu, D. C. Yan, and M. K. Wu, *Proc. Natl. Acad. Sci. USA* **105**, 14262 (2008).
 [10] Q.-Y. Wang, Z. Li, W.-H. Zhang, Z.-C. Zhang, J.-S. Zhang, W. Li, H. Ding, Y.-B. Ou, P. Deng, K. Chang, J. Wen, C.-L. Song, K. He, J.-F. Jia, S.-H. Ji, Y.-Y. Wang, L.-L. Wang, X. Chen, X.-C. Ma, and Q.-K. Xue, *Chin. Phys. Lett.* **29**, 037402 (2012).
 [11] D. Liu, W. Zhang, D. Mou, J. He, Y. B. Ou, Q. Y. Wang, Z. Li, L. Wang, L. Zhao, S. He, Y. Peng, X. Liu, C. Chen, L. Yu, G. Liu, X. Dong, J. Zhang, C. Chen, Z. Xu, J. Hu, X. Chen, X. Ma, Q. Xue, and X. J. Zhou, *Nature Commun.* **3**, 931 (2012).
 [12] S. N. Rebec, T. Jia, C. Zhang, M. Hashimoto, D.-H. Lu, R. G. Moore, and Z.-X. Shen, *Phys. Rev. Lett.* **118**, 067002 (2017).
 [13] S. He, J. He, W. Zhang, L. Zhao, D. Liu, X. Liu, D. Mou, Y. B. Ou, Q. Y. Wang, Z. Li, L. Wang, Y. Peng, Y. Liu, C. Chen, L. Yu, G. Liu, X. Dong, J. Zhang, C. Chen, Z. Xu, X. Chen, X. Ma, Q. Xue, and X. J. Zhou, *Nature Mater.* **12**, 605 (2013).
 [14] J. He, X. Liu, W. Zhang, L. Zhao, D. Liu, S. He, D. Mou, F. Li, C. Tang, Z. Li, L. Wang, Y. Peng, Y. Liu, C. Chen, L. Yu, G. Liu, X. Dong, J. Zhang, C. Chen, Z. Xu, X. Chen, X. Ma, Q. Xue, and X. J. Zhou, *Proc. Natl. Acad. Sci. USA* **111**, 18501 (2014).
 [15] X. Liu, D. Liu, W. Zhang, J. He, L. Zhao, S. He, D. Mou, F. Li, C. Tang, Z. Li, L. Wang, Y. Peng, Y. Liu, C. Chen, L. Yu, G. Liu, X. Dong, J. Zhang, C. Chen, Z. Xu, X. Chen, X. Ma, Q. Xue, and X. J. Zhou, *Nature Commun.* **5**, 5047 (2014).
 [16] Y. Miyata, K. Nakayama, K. Sugawara, T. Sato, and T. Takahashi, *Nature Mater.* **14**, 775 (2015).
 [17] J. J. Lee, F. T. Schmitt, R. G. Moore, S. Johnston, Y.-T. Cui, W. Li, M. Yi, Z. K. Liu, M. Hashimoto, Y. Zhang, D. H. Lu, T. P. Devereaux, D.-H. Lee, and Z.-X. Shen, *Nature (London)* **515**, 245 (2014).
 [18] S. Tan, Y. Zhang, M. Xia, Z. Ye, F. Chen, X. Xie, R. Peng, D. Xu, Q. Fan, H. Xu, J. Jiang, T. Zhang, X. Lai, T. Xiang, J. Hu, B. Xie, and D. Feng, *Nature Mater.* **12**, 634 (2013).
 [19] R. Peng, H. C. Xu, S. Y. Tan, H. Y. Cao, M. Xia, X. P. Shen, Z. C. Huang, C. H. P. Wen, Q. Song, T. Zhang, B. P. Xie, X. G. Gong, and D. L. Feng, *Nature Commun.* **5**, 5044 (2014).
 [20] W.-H. Zhang, Y. Sun, J.-S. Zhang, F.-S. Li, M.-H. Guo, Y.-F. Zhao, H.-M. Zhang, J.-P. Peng, Y. Xing, H.-C. Wang, T. Fujita, A. Hirata, Z. Li, H. Ding, C.-J. Tang, M. Wang, Q.-Y. Wang, K. He, S.-H. Ji, X. Chen, J.-F. Wang, Z.-C. Xia, L. Li, Y.-Y. Wang, J. Wang, L.-L. Wang, M.-W. Chen, Q.-K. Xue, and X.-C. Ma, *Chin. Phys. Lett.* **31**, 017401 (2014).
 [21] Y. Sun, W. Zhang, Y. Xing, F. Li, Y. Zhao, Z. Xia, L. Wang, X. Ma, Q.-K. Xue, and J. Wang, *Sci. Rep.* **4**, 6040 (2014).
 [22] W. Zhang, Z. Li, F. Li, H. Zhang, J. Peng, C. Tang, Q. Wang, K. He, X. Chen, L. Wang, X. Ma, and Q. K. Xue, *Phys. Rev. B* **89**, 060506(R) (2014).
 [23] J. Shiogai, Y. Ito, T. Mitsuhashi, T. Nojima, and A. Tsukazaki, *Nature Phys.* **12**, 42 (2016).

- [24] K. Hanzawa, H. Sato, H. Hiramatsu, T. Kamiya, and H. Hosono, *Proc. Natl. Acad. Sci. USA* **113**, 3986 (2016).
- [25] B. Lei, J. H. Cui, Z. J. Xiang, C. Shang, N. Z. Wang, G. J. Ye, X. G. Luo, T. Wu, Z. Sun, and X. H. Chen, *Phys. Rev. Lett.* **116**, 077002 (2016).
- [26] N. P. Ong, Z. Z. Wang, J. Clayhold, J. M. Tarascon, L. H. Greene, and W. R. McKinnon, *Phys. Rev. B* **35**, 8807 (1987).
- [27] J. Wu, O. Pelleg, G. Logvenov, Y.-J. Sun, G. S. Boebinger, M. Vanević, Z. Radović, and I. Božović, *Nature Mater.* **12**, 877 (2013).
- [28] G. R. Stewart, *Rev. Mod. Phys.* **83**, 1589 (2011).
- [29] H. Hosono and K. Kuroki, *Physica C* **514**, 399 (2015).
- [30] S. Kasahara, T. Watashige, T. Hanaguri, Y. Kohsaka, T. Yamashita, Y. Shimoyama, Y. Mizukami, R. Endo, H. Ikeda, K. Aoyama, T. Terashima, S. Uji, T. Wolf, H. von Löhneysen, T. Shibauchi, and Y. Matsuda, *Proc. Natl. Acad. Sci. USA* **111**, 16309 (2014).
- [31] J. Maletz, V. B. Zabolotnyy, D. V. Evtushinsky, S. Thirupathaiah, A. U. B. Wolter, L. Harnagea, A. N. Yaresko, A. N. Vasiliev, D. A. Chareev, A. E. Böhmer, F. Hardy, T. Wolf, C. Meingast, E. D. L. Rienks, B. Büchner, and S. V. Borisenko, *Phys. Rev. B* **89**, 220506(R) (2014).
- [32] Y. Ando, Y. Hanaki, S. Ono, T. Murayama, K. Segawa, N. Miyamoto, and S. Komiya, *Phys. Rev. B* **61**, 14956(R) (2000).
- [33] S. Ono, S. Komiya, and Y. Ando, *Phys. Rev. B* **75**, 024515 (2007).
- [34] X. Fan, W. Zheng, X. Chen, and D. J. Singh, *PLoS ONE* **9**, e91423 (2014).
- [35] K. Zou, S. Ismail-Beigi, K. Kisslinger, X. Shen, D. Su, F. J. Walker, and C. H. Ahn, *APL Mater.* **3**, 036104 (2015).
- [36] We note that the actual sign reversal in R_H occurs at $d \sim 3$ nm for KTaO_3 . This might be ascribed to the surface roughness of the FeSe film after a number of sequential etchings when the initial thickness is relatively thick. This also causes the scattered values of T_c^{on} for FeSe-EDLT on KTaO_3 substrate in Fig. 3(a).